Title

The Effect of Stress on Flow and Transport in Fractured Rock Masses Using an Extended Multiple Interacting Continua Method with Crack Tensor Theory

Journal

Nuclear Technology, 187(2)

ISSN

0029-5450

Authors

Wang, Zhen
Rutqvist, Jonny
Wang, Yuan
et al.

Publication Date

2014-08-01

DOI

10.13182/nt13-76

Peer reviewed

The Effect of Stress on Flow and Transport in Fractured Rock Masses Using an Extended Multiple Interacting Continua Method with Crack Tensor Theory

Zhen Wang[a, b], Jonny Rutqvist[a], Yuan Wang[a, c], Colin Leung[d], Andrew Hoch[d], Ying Dai[b]

[a]Earth Science Division, Lawrence Berkeley National Laboratory (LBNL), Berkeley, CA 94720 USA

[b]School of Aerospace Engineering and Applied Mechanics, Tongji University, Shanghai 200092, China

[c]Hohai University, Nanjing, China

[d]AMEC, Didcot, UK

Name: Zhen Wang

E-mail: wangzhen_hn@hotmail.com

Mailing Address: Room 309, East Building, 100 Zhangwu Road, Shanghai 200092, China

Number of pages: 25

Number of tables: 2

Number of figures: 10

This paper is part of the TOUGH2 special issue

Abstract: We present an extended multiple interacting continua (Ex-MINC) model of fractured rock masses that uses Oda's crack tensor theory to upscale the hydraulic and mechanical properties. The Ex-MINC concept includes separate connected continua representing active-fractures, inactive-fractures, and matrix to represent the fracture-matrix system. The crack tensor theory was used to calculate the stress-dependent permeability tensor and compliance tensor for individual grid blocks. By doing this, we transformed a discrete fracture network model into a grid-based continuum model. The Ex-MINC model was verified against an existing analytical solution and the entire Ex-MINC /crack-tensor model approach was applied to a benchmark test related to coupled stress, fluid flow and transport through a 20 × 20 m model domain of heavily fractured media. This benchmark test was part of the international DECOVALEX project for the development of coupled models and their validation, thus providing us with the opportunity to compare our results with the results of independent models. We conducted the coupled hydraulic and mechanical modeling with TOUGH-FLAC, a simulator based on the TOUGH2 multiphase flow code and the FLAC3D geomechanical code. The results of our simulations were generally consistent with the results of the other independent modeling approaches, and showed how inactive fractures impeded solute transport through the fractured system by providing an additional fracture surface area as an avenue for increasing fracture-matrix diffusion.

Keywords: fractured rock, extended multiple interacting continua method, crack tensor theory

I INTRODUCTION

Coupled hydromechanical effects, such as the effect of stress on permeability, could have a significant impact on flow and transport in fractured rock[1]. These are complex processes that can be studied using numerical modeling, although not without encountering difficulties related to upscaling and deriving representative values for both mechanical and hydrological parameters. In this study, we present an extended multiple interacting continua (Ex-MINC) model, which uses Oda's crack tensor theory[2] to upscale the hydraulic and mechanical properties determined from a discrete-fracture-network model. The fracture-matrix system can be conceptualized into three parts: (1) active fractures, which are fractures or part of fractures connected globally and dominate the fluid flow and solute transport; (2) inactive fractures, which are "dead-end" parts of original fractures and do not contribute significantly to fluid flow; and (3) matrix, including isolated fractures, which here are considered as part of the matrix. The Ex-MINC model (including separate and connected continua representing active-fractures, inactive-fractures and matrix) extends the "multiple interacting continua" (MINC) method[3] by adding one more inactive-fracture continuum. The crack tensor theory was used to calculate the stress-dependent permeability tensor and compliance tensor for individual grid blocks. Using this modeling approach, the discrete fracture network was transformed into a grid-based continuum model. We implemented this modeling approach into the framework of TOUGH-FLAC[4,5], a simulator that links the TOUGH2[6] multiphase fluid flow code with the FLAC3D[7] geomechanical code.

We applied this methodology to a 2D Bench Mark Test (BMT) problem, defined and analyzed within

the international DECOVALEX project[8,9]. The BMT consists of a 20 × 20 m model domain with a 2D fracture-network model (Fig. 1a) composed of 7797 individual fractures whose apertures are correlated to their lengths. The effects of stress and hydraulic pressure gradients are considered through various boundary conditions (Fig. 1).

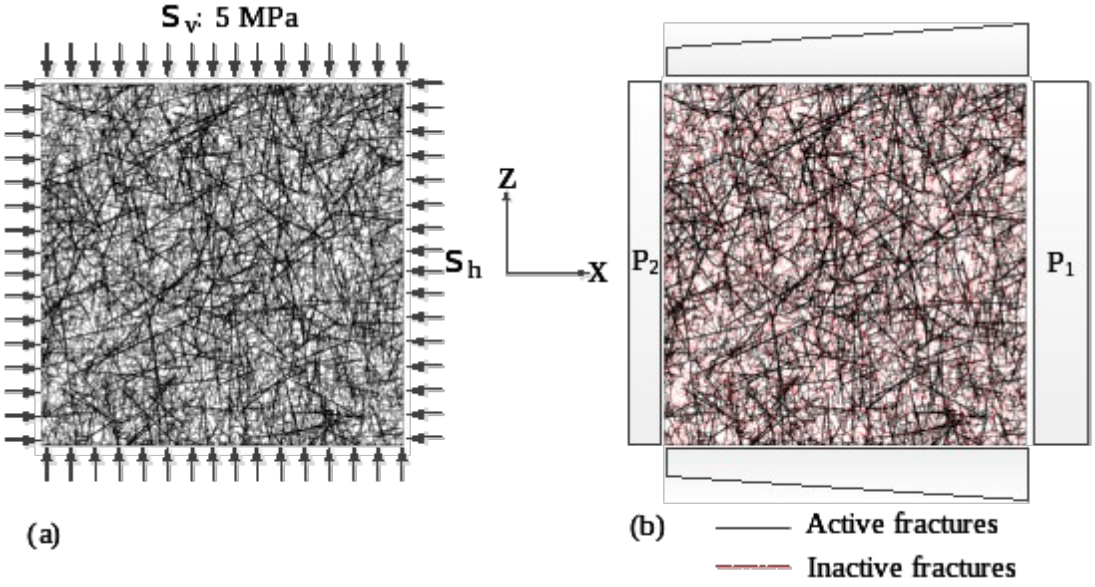

Fig. 1. 2-D BMT fracture network. (a) Original fracture network under mechanical boundary conditions; (b) Connected fracture network (solid line) with inactive fractures (dashed line) under hydraulic boundary conditions.

For the mechanical boundary conditions, we specified a constant vertical stress σ_v of 5 MPa at the top and bottom surfaces, whereas a varying horizontal stress σ_h was specified at the right- and left-hand side boundaries to cause different fracture shear behaviors inside the model (Fig. 1a). The horizontal stress had increasing magnitude, corresponding to the stress ratio (K) of horizontal/vertical stress, varying from 1,2,3,5, to progressively induce shear failure along fractures within the model.

For each set of the stress boundary conditions (once the model is in an equilibrium state), fluid flow and transport through the model was simulated by the specific hydraulic boundary conditions

representing a hydraulic gradient P_1-P_2 (Fig. 1b). For such hydraulic boundary conditions, a constant pressure gradient of either 1.0×10^4 Pa/m and 10 Pa/m was simulated.

The mechanical properties of the rock matrix and fractures are listed in Table I. For simplicity, mechanical and hydraulic apertures are assumed to be equal.

Table I
Model properties of intact rock and fractures

	Properties	value
Intact rock	Elastic modulus, E (GPa)	84.6
	Poisson's ratio, υ	0.24
Fractures	Shear stiffness, K_s (GPa/m)	434
	Friction angle, φ (°)	24.9
	Dilation angle, d (°)	5
	Cohesion, c (MPa)	0
	Critical shear displacement for dilation, U_{cs} (mm)	3
	Minimum aperture value, a_{res} (μm)	1
	Maximum aperture value, a_{max} (μm)	200

II METHODOLOGY

II.A Extended Multiple Interacting Continua Model

Fig. 2c illustrates the Ex-MINC modeling concept, which is compared with the MINC method (Fig. 2b), and a triple-continuum concept[10] (Fig. 2a). The above three modeling concepts are inspired by and adopt features of the classical dual continuum approach[11] involving a continuum treatment for both the fracture network and the porous rock matrix. The Ex-MINC method involving inactive fractures extends the MINC concept (Fig. 2b) by adding one more connection (via the inactive-fracture continuum) between the active-fracture continuum and the matrix continuum (Fig. 2c), which is similar to the triple-continuum concept (Fig. 2a). However, differences exist between Ex-MINC and triple-

continuum models. The triple-continuum is an extension of the dual-permeability model, which can consider both fracture-fracture and matrix-matrix flow, but limited to a quasi-steady fracture-matrix flow; while the Ex-MINC model can simulate transient fracture-matrix flow. Besides, the triple-continuum model uses two sets of fracture geometric parameters such as fracture spacings for active and inactive fractures respectively; while the Ex-MINC model considers active and inactive fractures as part of one pattern of fractures, and therefore uses only one fracture spacing. Thus, the Ex-MINC model partitions the fracture-matrix system into three kinds of continua: active-fracture, inactive-fracture and nested matrix continua. Using these three continua and their connections, the Ex-MINC approach can handle active fracture-matrix (F-M) interactions, inactive fracture-matrix (f-M) interactions, and active fracture-inactive fracture (F-f) interactions.

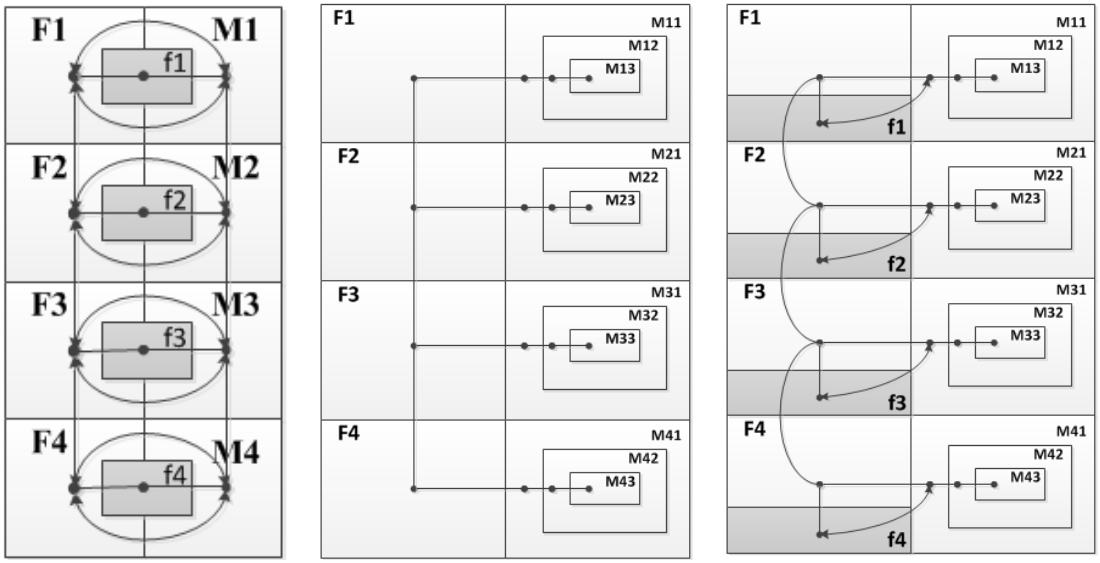

(a) (b) (c)

Fig. 2. Schematic of different conceptualizations for partitioning a fracture-matrix system: (a) Triple-continuum model; (b) MINC model; (c) Ex-MINC model. (M=matrix; F=Active fractures; f=inactive fractures). Modified from Ref. 10 and Ref. 12.

The Ex-MINC method follows the same partitioning scheme as the MINC method except for the determination of intra-block connections (interface area $A_{F\text{-}f}$ and nodal distance $D_{F\text{-}f}$) between the active-fracture continuum and the inactive-fracture continuum. More details about the partitioning scheme of the MINC method can be found in Ref. 3, Ref. 13 and Ref. 14. Here we assume that each original fracture has a part that could be classified as an inactive fracture and introduce a characteristic length (l_f) of the inactive fractures. With our detailed 2-D fracture network the characteristic length (l_f) can be obtained from the ratio of the total inactive-fracture area to the sum of original fracture apertures. The sum of original fracture apertures is also considered to give the interface area ($A_{F\text{-}f}$), and we take half of the characteristic length (l_f) as the nodal distance ($D_{F\text{-}f}$).

The fracture spacing is determined by the criterion that arbitrarily distributed fractures can be idealized to be two orthogonal sets of plane parallel fractures or one set of plane parallel fractures with the same fracture intensity P32, where P32 is defined as the fracture surface area per unit volume.

II.B Oda's Crack Tensor Theory

According to the BMT definition, the normal stiffness of a single fracture is linked to the normal stress and initial fracture aperture by Ref. 15.

$$K_n = \frac{(10\sigma_n + \sigma_{nc})^2}{9\sigma_{nc} b_0} \qquad (1)$$

where σ_n is the normal stress across the fracture, b_0 is the initial aperture, and σ_{nc} is the critical normal stress defined as σ_{nc} [MPa] = 0.487 × b_0 [μm] + 2.51. Moreover, in the BMT definition a constant shear stiffness of K_s=434 GPa was defined for simplicity (Table. I).

The anisotropy of the permeability and elastic stiffness were obtained using Oda's crack tensor theory[2], formulated as a discrete summation of contributions from each fracture that intersect an element volume. We could apply this discrete summation approach because the description of fractures given by the BMT definition is explicit (each fracture is known by its position and its geometric properties – length, orientation, and aperture). The basic quantities of the crack tensor for each crack in an element are as follows:

$$F_{ij} = \frac{1}{V_e}\frac{\pi}{4} D^3 n_i n_j \qquad (2)$$

$$F_{ijkl} = \frac{1}{V_e}\frac{\pi}{4} D^3 n_i n_j n_k n_l \qquad (3)$$

$$P_{ij} = \frac{1}{V_e}\frac{\pi}{4} D^2 b^3 n_i n_j \qquad (4)$$

where F_{ij}, F_{ijkl}, P_{ij} are the basic crack tensors, V_e is the element volume, D is the equivalent diameter of the crack, b is the aperture of the crack, and **n** is the unit vector of normal orientation for each crack with components n_i (i=1,2,3).

By using the above quantities and the mechanical properties for each fracture, we calculated the anisotropic compliance tensor C_{ijkl} and the permeability tensor k_{ij} using

$$C_{ijkl} = \sum^{NCR} [(\frac{1}{K_n D} - \frac{1}{K_s D})F_{ijkl} + \frac{1}{4K_s D}(\delta_{ik}F_{jl} + \delta_{jk}F_{il} + \delta_{il}F_{jk} + \delta_{jl}F_{ik})] \qquad (5)$$

$$k_{ij} = \sum^{NCR} \frac{1}{12}(P_{kk}\delta_{ij} - P_{ij}) \quad (6)$$

where NCR is number of cracks in an element, and δ_{ij} is Kronecker's delta. The total elastic compliance tensor can be formulated as

$$T_{ijkl} = C_{ijkl} + M_{ijkl} \quad (7)$$

$$M_{ijkl} = (1/E)[(1+\nu)\delta_{ik}\delta_{jl} - \nu\delta_{ij}\delta_{kl}] \quad (8)$$

where M_{ijkl} is the elastic compliance tensor of the intact rock.

The stress dependent permeability tensor is calculated by considering only the active fractures since the inactive fractures do not contribute significantly to fluid flow. The stress dependent compliance tensor, on the other hand, is determined with contributions from all of the original fractures (active, inactive and isolated fractures) because they will increase the compliance of the intact rock and the fractured rock mass as a whole.

II.C Stress/aperture Coupling Considering Shear Dilation

The effect of stress on the permeability tensor was evaluated for each element by considering the stress-induced aperture changes for each fracture intersecting the element. The stress-induced aperture change is expressed as follows[15]:

$$b = b_0 - \delta + \Delta b_{dil} \quad (9)$$

$$\delta = \frac{9\sigma_n b_0}{\sigma_{nc} + 10\sigma_n} \quad (10)$$

where δ is the normal closure caused by an increase in normal stress, and Δb_{dil} is the dilatational normal displacement associated with fracture shear slip. Eq. (10) displays the typical nonlinear normal stress/aperture relationship for rock fractures[15].

The approach for modeling shear dilation is shown in Fig. 3. If the shear stress τ on a fracture is below the critical shear stress τ_{cs} (Region 1), no shear-induced normal displacement occurs. When the shear stress is larger than the critical shear stress (Region 2), slip occurs, and the fracture shear stiffness in Region 2 is calculated as

$$K_{s2} = \eta \frac{G}{r} \tag{11}$$

where G is the shear modulus of the intact rock, r is the radius of the fracture, and η is a factor with a value that depends upon the geometry of the slip patch[8]. In our case, we may consider a circular crack in which η=7π/24. Thus, the dilatational normal displacement can be calculated using

$$\Delta b_{dil} = \frac{\tau - \tau_{cs}}{K_{s2}} \cdot \tan(d) \tag{12}$$

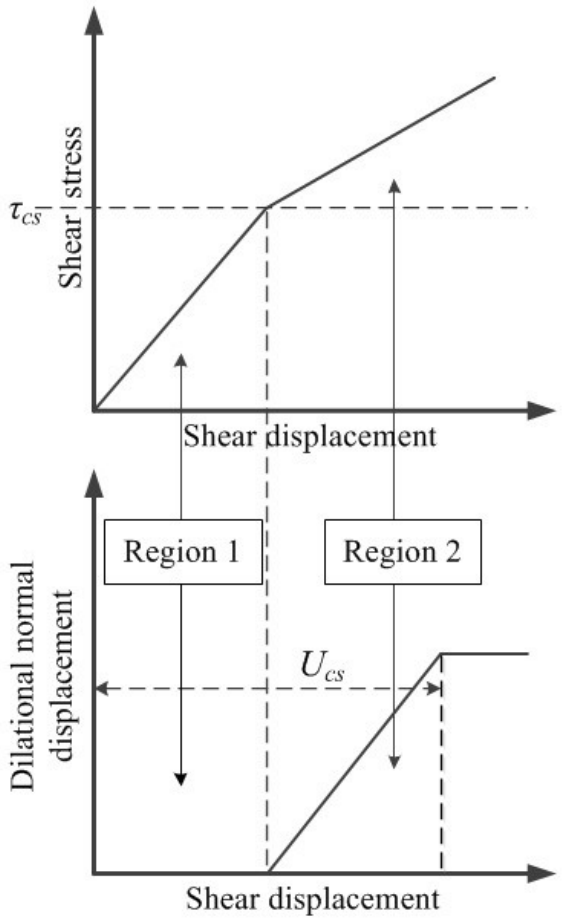

Fig. 3. Strategy for modeling shear dilation

II.D Calculation Procedure

The original fractures are first categorized into active, inactive and isolated fractures. When the model domain is in free stress state (i.e. stress ratio K=0), we can use the fracture geometry and mechanical information to calculate the initial total elastic compliance tensor (determined by original fractures), permeability tensor (determined by active fractures) and Ex-MINC model parameters (determined by active and inactive fractures). When the stress ratio K=1, we first assign an initial total elastic compliance tensor to each element in the FLAC3D model (employing a user-defined elastic anisotropic constitutive model) and calculate the new stress state. Note that because of the

heterogeneous compliance within the model, with different compliance tensors for each element, the new stress state will be heterogeneous, somewhat different from the stress applied at the model boundaries. Then, we use the new stress field to calculate the stress-induced fracture changes and update the permeability and compliance tensors and Ex-MINC model parameters for each element. With the permeability tensor defined in each element, we use TOUGH2/Ex-MINC to simulate the flow and transport through the model. The same procedures are used for the stress ratios K=2, 3, and 5. Consequently, with K increasing from 0 to 5, the elastic stiffness and permeability tensors are updated anisotropically in each element and heterogeneously over the model domain. The flowchart of this procedure and calculation algorithm using TOUGH-FLAC is shown in Fig. 4.

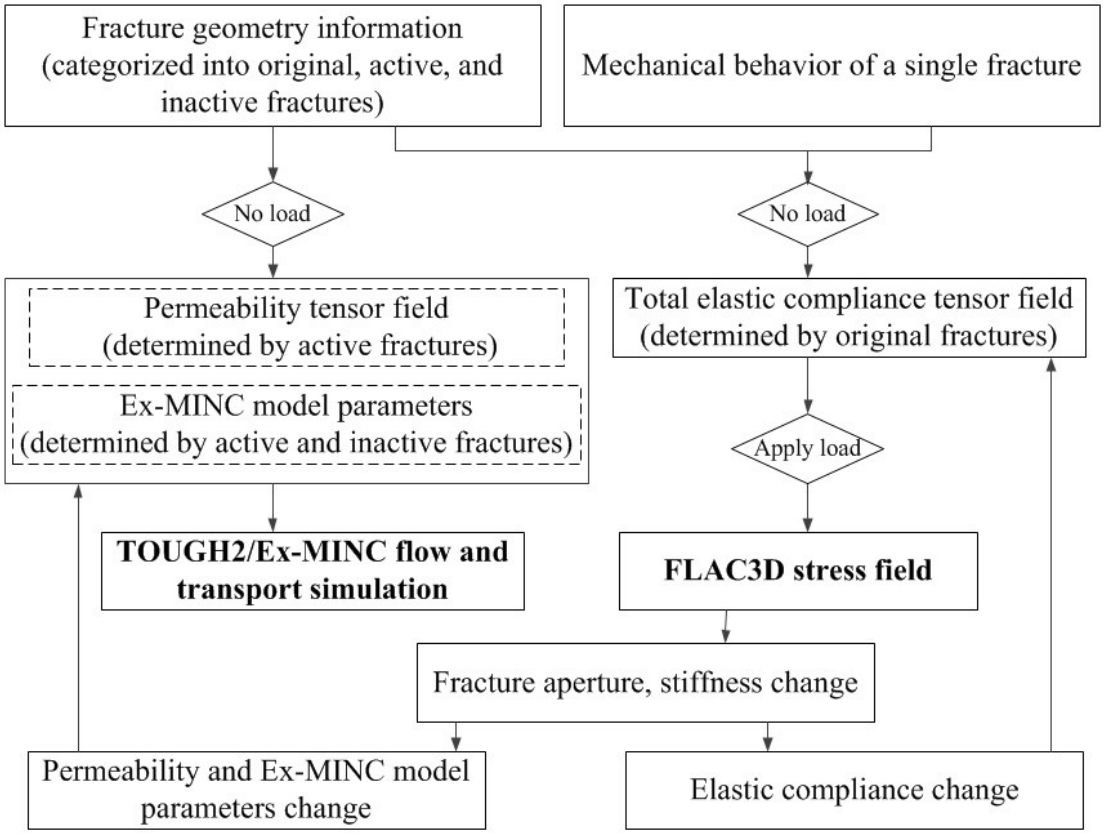

Fig. 4. Flowchart of the calculation algorithm

III A VERIFICATION PROBLEM OF Ex-MINC METHOD

In this section, the Ex-MINC model is applied to a wellbore flow problem that was defined and analyzed both analytically and numerically in Ref. 10. The problem under consideration involves one-dimensional radial flow into a fully penetrating well in a radially infinite, horizontal reservoir that contains a uniform fracture system (including active and inactive fractures) and matrix. Neglecting consideration of wellbore storage and skin effects, Ref. 16 and Ref. 10 presented an analytical solution for the dimensionless pressure drop at the wellbore assuming a triple-porosity model. The basic parameters for the analytical solution and the derived model parameters for the Ex-MINC model are

listed in Table. II. The derived Ex-MINC model parameters such as fracture spacing (matrix block size) and characteristic length of inactive fractures are determined from the given inter-porosity flow shape factor α by using the Warren-Root pseudo-steady state model[11].

Table II

Parameters used in the wellbore flow problem using either a triple-porosity model or an Ex-MINC model of the fractured reservoir

	Parameter	Value	Unit
Basic parameters	Matrix porosity	$\phi_M = 0.263$	
	Active fracture porosity	$\phi_F = 0.001$	
	Inactive fracture porosity	$\phi_f = 0.01$	
	Matrix permeability	$k_M = 1.572\times10^{-16}$	m^2
	Active fracture permeability	$k_F = 1.383\times10^{-12}$	m^2
	Inactive fracture permeability	$k_f = 1.383\times10^{-14}$	m^2
	Total compressibility of three media	$C_M=C_F=C_f= 1.0\times10^{-9}$	1/Pa
	Well radius	$r_w = 0.1$	m
	Well production rate	$q = 100$	m^3/day
	Formation thickness	$h = 20$	m
	F-M shape factor	$\alpha_{F-M} = 0.480$	m^{-2}
	F-f shape factor	$\alpha_{F-f} = 0.351$	m^{-2}
	f-M shape factor	$\alpha_{f-M} = 4.688$	m^{-2}
	Water density	$\rho =1000$	kg/m^3
	Water phase viscosity	$\mu =1\times10^{-3}$	Pa·s
Derived model parameters	Fracture spacing	$FS = 1.5$	m
	f characteristic length	$l_f = 0.24$	m

Fig.5 shows the evolution of the pressure drawdown at the wellbore, comparing numerical and analytical solutions. The pressure drawdown curve for the Ex-MINC model with three continua (one active-fracture continuum, one inactive-fracture continuum and one matrix continuum, circles) is in good agreement with the analytical solution for the triple-porosity model (solid line), and exhibits three distinct, straight, parallel lines in semi-log space which reflects the effect of active, inactive fractures

and matrix on fluid flow in this order as time increases. Applying an Ex-MINC model with ten continua (two fracture continua and eight matrix continua, dashed line in Fig. 5) results in a smoother pressure drop at intermediate times, because sub-gridding the matrix block can be used to represent the fracture-matrix interaction in a fully transient way, while the Ex-MINC model with three continua is limited to quasi-steady state inter-continuum fracture-matrix flow.

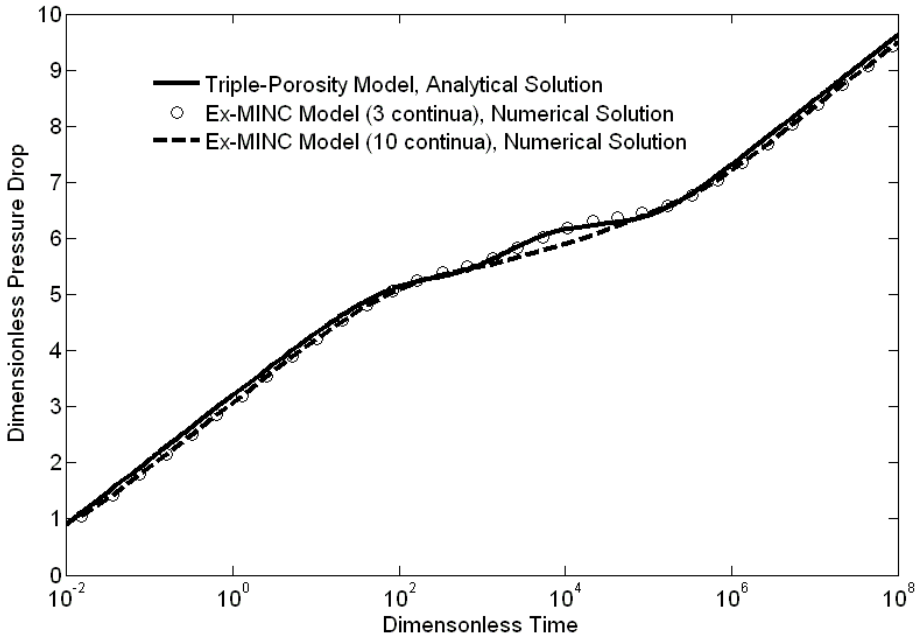

Fig. 5. Comparison of pressure drawdown curves between numerical and analytical solutions.

According to Ref. 10, in practice, the complete triple-porosity model parameters, such as porosity, permeability, compressibility and shape factors between different continuum, could be determined by combining well-pumping (or injection) test and tracer tests with field (e.g. fracture mapping) and laboratory (e.g. matrix properties) studies. Then we can derive our Ex-MINC model parameters through the basic triple- porosity model parameters.

IV RESULTS AND DISCUSSION OF 2-D BMT PROBLEM

The Ex-MINC model was incorporated into TOUGH2 to perform the fluid flow and transport simulation, which accounts for rock-matrix diffusion and the effect of inactive fractures. Apply the Ex-MINC/crack tensor approach to the 2D benchmark test of the international DECOVALEX project, we divided the model domain into 40×40 elements of side length 0.5 m. Such a cell size makes sure that each block has enough fractures to behave like a continuum, and the total number of elements is large enough to reduce the effect of numerical dispersion in modeling solute transport[8]. TOUGH-FLAC simulation results (denoted as LBNL) were compared with the simulation results obtained by three other teams using different modeling approaches. The IC team used the discrete fracture network (DFN) NAPSAC model and a particle tracking method for simulating solute transport; the KTH team used the distinct element code UDEC and a particle tracking method, and the TUL team used a combined DFN and equivalent continuum flow and solute transport code FLOW123D. The approaches and results of other teams are described in Ref. 9.

We used the flow rate at the downstream outlet to calculate the equivalent model-domain permeability. The resulting equivalent model-domain permeability decreases with increasing stress ratio. Moreover, the equivalent vertical permeability decreases more than the equivalent horizontal permeability when the horizontal stress is increased while the vertical stress is kept constant (Fig. 6).

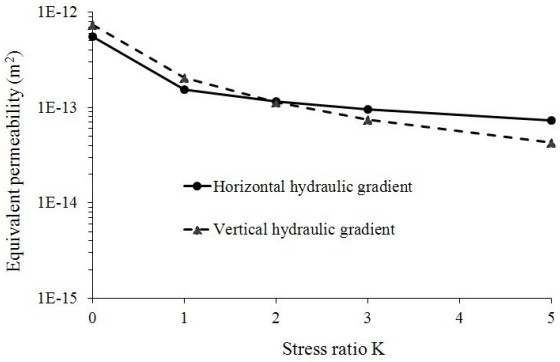

Fig. 6. Equivalent permeability for horizontal and vertical flow at different stress ratios.

For the transport calculation, we used a solute transport approach, which can be described as follows: (1) initially the concentration over the entire model is zero; (2) then there is a short interval of constant concentration at the inlet boundary; (3) and thereafter there is zero concentration inflow along all of the boundaries, including the lateral sides parallel to the global flow direction.

Under a relatively high hydraulic pressure gradient of 10^4 Pa/m, advection is the main "driving force" of solute transport. The simulation results for the case of horizontal flow under this relatively high horizontal gradient are compared in terms of breakthrough curves in Fig. 7. When K=0 (Fig. 7a), the breakthrough curves calculated by the four teams are quite similar. When considering the effects of an applied load (Fig. 7b-d), the four teams predict a general trend involving a shift of the breakthrough curves towards longer time with increasing stress ratios, but some differences between the breakthrough curves can be observed. In general, the results of our Ex-MINC and solute transport approach are very similar to those obtained by TUL, even under increasing mechanical load. The results of KTH and IC indicate a relatively slower breakthrough under increasing load. It is not clear what causes this systematic difference in the breakthrough, because according to Ref. 8, the equivalent

permeability and total flow through the model domain are very similar for the different approaches. It appears that the two teams (KTH and IC) which used particle tracking obtained a delayed breakthrough compared to the two teams (LBNL and TUL) which used standard solute-transport models.

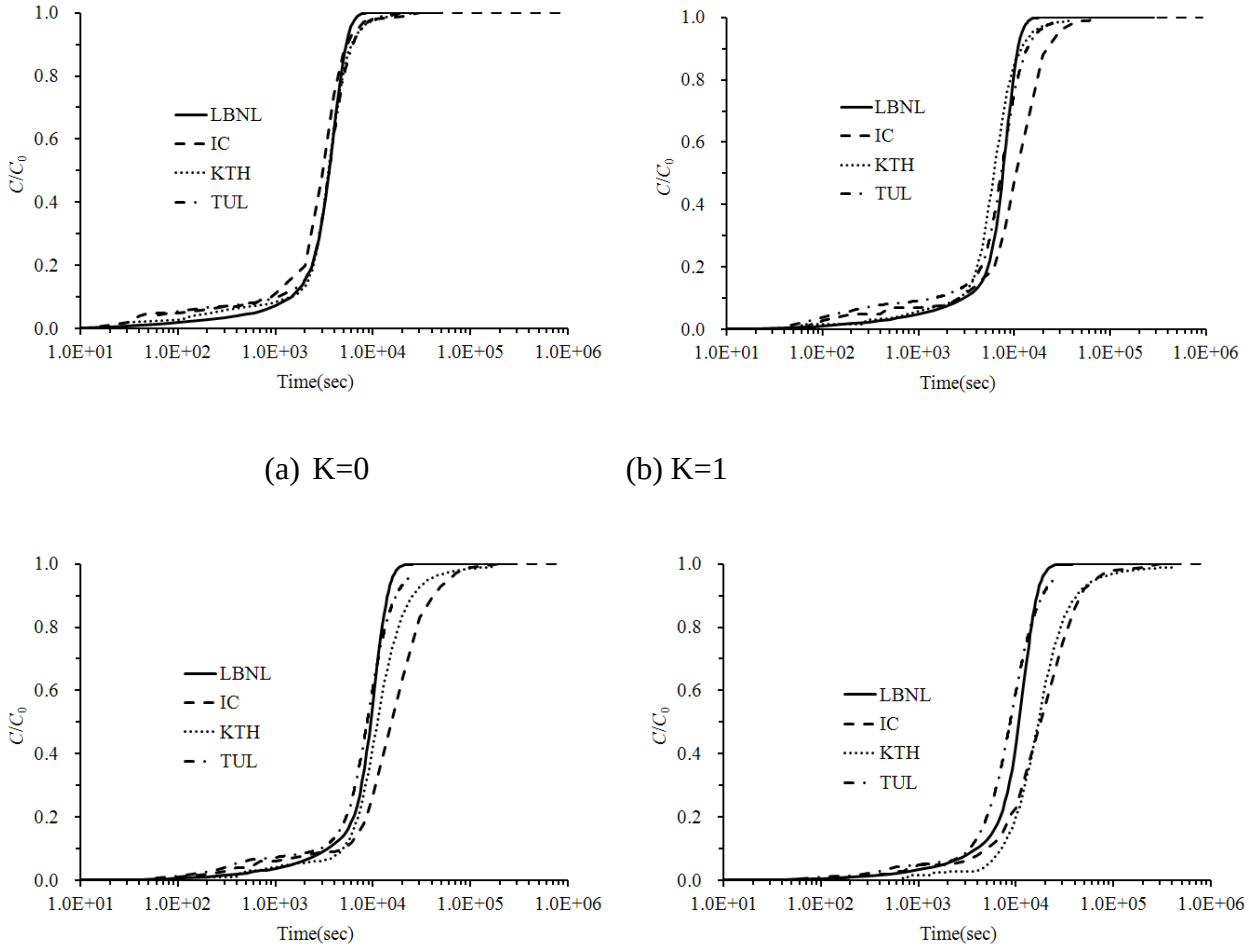

(a) K=0 (b) K=1

(c) K=3 (d) K=5

Fig. 7. Comparison of breakthrough curves for solute that can exit from three outlet boundaries at increasing stress ratios, under a horizontal hydraulic gradient of 10^4 Pa/m

The process of rock-matrix diffusion has an important influence on transport behaviour under low hydraulic gradients (10 Pa/m) (Fig. 8). The general trend of breakthrough curves shifting to later time with increasing stress ratios in Fig. 8 is consistent with the high hydraulic gradient case shown in Fig.

7. The much longer tails for the breakthrough curves when accounting for rock-matrix diffusion indicate that a portion of solute could reside in the matrix micro-pores for a long time before diffusing back to the fractures. Consequently, under a low hydraulic gradient, rock-matrix diffusion will impede solute transport through the system. As shown in Fig. 9, when the stress ratio increases, more solute will diffuse into the matrix, and as a result, solute transport will be strongly retarded. This contrasts with the high hydraulic pressure gradient case, for which a negligible amount of solute diffuses into the rock matrix no matter what the stress state is (these results are not shown in figures).

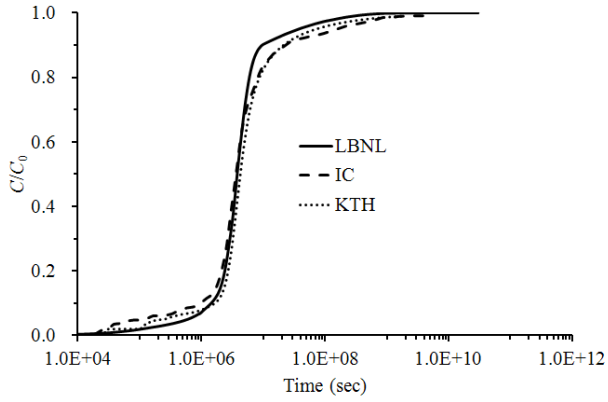

(a) K=0

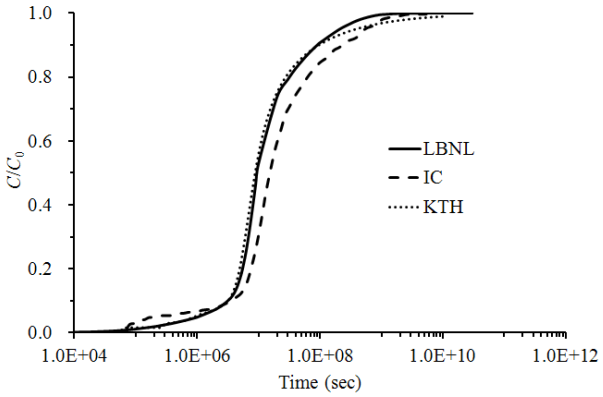

(b) K=1

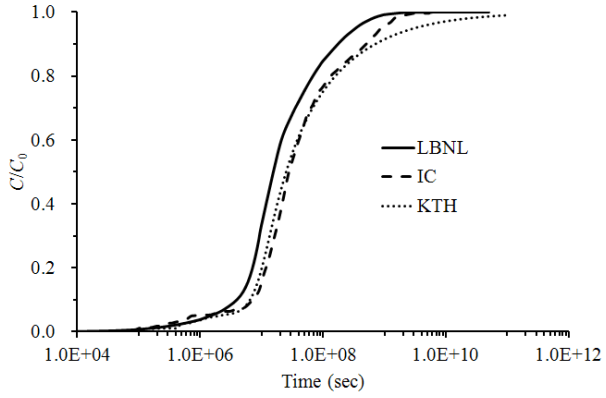

(c) K=3

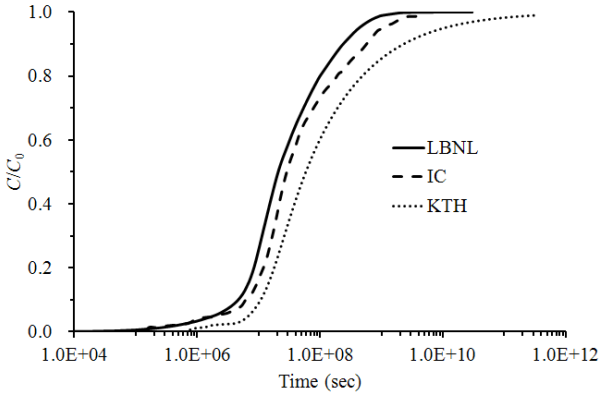

(d) K=5

Fig. 8. Comparison of breakthrough curves for solute that can exit from three outlet boundaries at increasing stress ratios, under a horizontal hydraulic gradient of 10 Pa/m

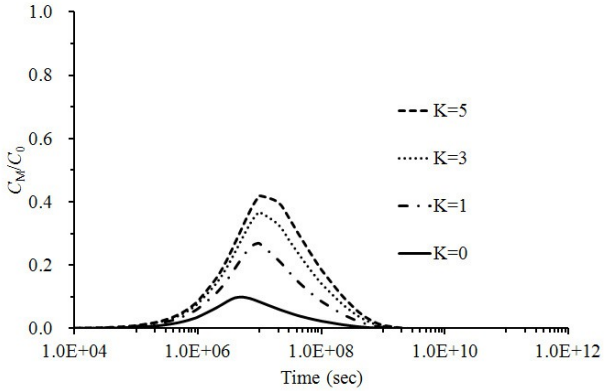

Fig. 9. Variation of the solute concentration in the rock matrix for increasing stress ratios K=0 to 5, under a horizontal hydraulic gradient of 10 Pa/m.

The effect of inactive fractures on solute transport is investigated by comparing solute concentration evolution in the rock matrix (Fig. 10a) and breakthrough curves (Fig. 10b) between the Ex-MINC model and the active-fracture model when stress ratio is K=5 and the hydraulic pressure gradient is low (10 Pa/m). In the active-fracture model we did not consider the effect of inactive fractures, but we did use the same permeability tensor field (determined from the connected fracture network) as in the Ex-MINC model. The comparison of the results in Fig. 10 indicates that the inactive fractures can enhance rock-matrix diffusion (Fig. 10a) and hence impacts the overall solute transport behavior (Fig. 10b). This enhancement of rock-matrix diffusion is due to that inactive fractures provide additional fracture-matrix contact area as an avenue for mass exchange between fractures and matrix. The inactive fractures although contribute little to fluid flow, can have a significant impact on the solute transport through enhancing rock-matrix diffusion. This enhancement of matrix diffusion through inactive fractures in a 2-D fracture network is also consistent with the findings of multi-process matrix diffusion

in field tracer tests in Ref. 17.

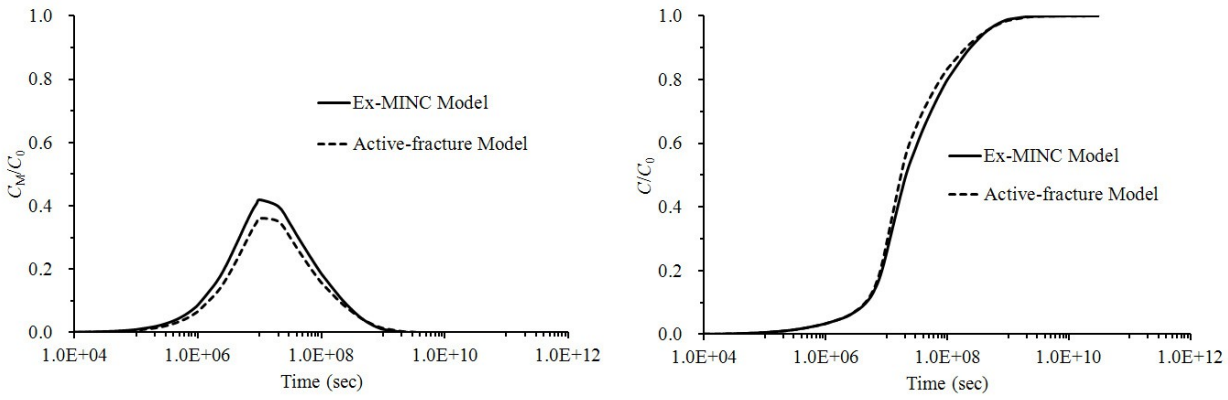

(a) (b)

Fig. 10. A comparison between the Ex-MINC model and the active-fracture model: (a) evolution of solute concentration in the rock matrix; (b) Breakthrough curves.

V CONCLUDING REMARKS

In this paper, we presented an investigation related to stress effects on fluid flow and transport in fractured rock masses. In particular, we used an Ex-MINC method and effective properties derived using Oda's crack tensor theory, and accounted for inactive fractures. We verified the Ex-MINC model against analytical and numerical simulation results for a well test problem in a fractured media and we applied the entire Ex-MINC/crack tensor approach to a 2D benchmark test defined and analyzed in the international DECOVALEX project. Results were compared with other independent modeling approaches, including discrete fracture models, and generally showed good agreement, and these inter-model comparisons build confidence in modeling stress effects on flow and transport in fractured media, especially since our Ex-MINC/crack tensor approach could be readily applied for studying large-scale coupled processes in three dimensions. Further, model development work undoubtedly must

continue due to the discrepancies observed at higher stresses and requirement of calibration to the real-world applications.

Some basic understanding of stress effects on flow and transport in fractured rocks can also be drawn:

1. When the compressive stress increase, fractures apertures close, resulting in a reduction of permeability and porosity. Solute transport is significantly retarded as a result of this permeability reduction.

2. Under a low hydraulic gradient, rock-matrix diffusion becomes increasingly important and significantly impedes the solute transport.

3. Inactive fractures, although contributing little to total fluid flow through the system, do increase the contact areas between fracture and matrix systems. This enhances rock-matrix diffusion, and thereby impacts the overall solute transport behavior.

In this paper, we applied a sequential coupled stress-flow-transport model, in which we considered the effects of stress on permeability, but not the effects of pore fluid pressure on fracture deformation. The one-way coupled approach is justifiable in this case, because the fluid pressure is very small compared to the applied stress. However, our approach can be readily extended and applied to two-way coupled problems, and this possibility will be the subject of future studies.

Acknowledgement

The first author would like to acknowledge the financial supports from the National Basic Research Program of China (973 Program: 2011CB013800) and the China Scholarship Council (CSC). Financial

support was also provided by the UK Nuclear Decommissioning Authority (NDA) to Lawrence Berkeley National Laboratory through the National Energy Technology Laboratory, under the U.S. Department of Energy Contract No. DE-AC02-05CH11231.

References

1. J. RUTQVIST and O. STEPHANSSON, "The Role of Hydromechanical Coupling in Fractured Rock Engineering," *Hydrogeology Journal*,**11**, 7 (2003).

2. M. ODA, "An Equivalent Continuum Model for Coupled Stress and Fluid-Flow Analysis in Jointed Rock Masses," *Water Resources Research*, **22**, 1845 (1986).

3. K. PRUESS and T. N. NARASIMHAN, "A Practical Method for Modeling Fluid and Heat-Flow in Fractured Porous-Media," *Society of Petroleum Engineers Journal*, **25**, 14 (1982).

4. J. RUTQVIST, Y. S. WU, C. F. TSANG, and G. BODVARSSON, "A Modeling Approach for Analysis of Coupled Multiphase Fluid Flow, Heat Transfer, and Deformation in Fractured Porous Rock," *International Journal of Rock Mechanics and Mining Sciences*, **39**, 429 (2002).

5. J. RUTQVIST, "Status of the TOUGH-FLAC Simulator and Recent Applications Related To Coupled Fluid Flow and Crustal Deformations," *Computers & Geosciences*, **37**, 739 (2011).

6. K. PRUESS, C. M. OLDENBURG, and G. J. MORIDIS, "TOUGH2 User's Guide Version 2," Tech. Rep. LBNL-43134, Lawrence Berkeley National Laboratory (1999).

7. "FLAC3D Fast Lagrangian Analysis of Continua in 3 Dimensions. Version 3.1," MInneapolis, MInnnesota, Itasca Consulting Group (2006).

8. J. RUTQVIST, C. LEUNG, A. HOCH, Y. WANG, and Z. WANG, "Linked Multicontinuum and Crack Tensor Approach For Modeling of Coupled Geomechanics, Fluid Flow and Transport in Fractured Rock," *Journal of Rock Mechanics and Geotechnical Engineering*, **5**, 18 (2013).

9. Z. ZHAO, J. RUTQVIST, C. LEUNG, M. HOKR, Q. LIU, I. NERETNIEKS, A. HOCH, J.

HAVLÍČEK, Y. WANG, Z. WANG, Y. WU, and R. ZIMMERMAN, "Impact of Stress on Solute Transport in a Fracture Network: A Comparison Study," *Journal of Rock Mechanics and Geotechnical Engineering*, **5**, 110 (2013).

10. Y.-S. WU, H. H. LIU, and G. S. BODVARSSON, "A Triple-Continuum Approach for Modeling Flow and Transport Processes in Fractured Rock," *Journal of Contaminant Hydrology,* **73**, 145 (2004).

11. J. E. WARREN and P. J. ROOT, "The Behavior of Naturally Fractured Reservoirs," *Society of Petroleum Engineers Journal*, **3**, 245 (1963).

12. C. DOUGHTY, "Investigation of Conceptual and Numerical Approaches for Evaluating Moisture, Gas, Chemical, and Heat Transport in Fractured Unsaturated Rock," *Journal of Contaminant Hydrology,* **38**, 69 (1999).

13. K. PRUESS and K. KARASAKI, "Proximity Function for Modeling Fluid and Heat Flow in Reservoirs with Stochastic Fracture Distributions," *Proceedings Eighth Workshop Geothermal Reservoir Engineering*, pp. 220-224, Standford University, Standford, CA, December 1982.

14. K. PRUESS, "GMINC- A Mesh Generator for Flow Simulations in Fractured Reservoirs," Tech. Rep. LBNL-15227, Lawrence Berkeley National Laboratory (1983).

15. A. BAGHBANAN and L. JING, "Stress Effects on Permeability in a Fractured Rock Mass with Correlated Fracture Length and Aperture," *International Journal of Rock Mechanics and Mining Sciences*, **45**, 1320 (2008).

16. J. LIU, G. S. BODVARSSON, and Y.-S. WU, "Analysis of Flow Behavior in Fractured Lithophysal Reservoirs," *Journal of Contaminant Hydrology,* **62**, 189 (2003).

17. Q. ZHOU, H-H. LIU, G. S. BODVARSSON and F. J. MOLZ, “Evidence of Multi-process Matrix Diffusion in a Single Fracture form a Field Tracer Test,” *Transport in Porous Media*, **63**, 473 (2006).